JOURNAL OF AIRCRAFT
Vol. 32, No. 1, January–February 1995

Natural Laminar Flow Wing Concept for Supersonic Transports

Berry T. Gibson* and Heinz A. Gerhardt†
Northrop Grumman Corporation, Pico Rivera, California 90660

A "reverse" delta wing, having a straight leading edge and forward-swept trailing edges, is shown to be capable of achieving extended runs of natural laminar flow during supersonic flight. Euler calculations at supersonic Mach number confirm that the flow over a reverse delta wing is nominally two dimensional, in contrast to delta wing flow that exhibits large spanwise flow gradients, particularly near the leading edge. The data suggest that crossflow and attachment line instabilities, the primary modes of transition on swept wings, are minimal on a reverse delta wing. Predicted forces on 2% thick delta and reverse delta wings are in accord with the principles of reciprocal flow theory because lift-curve slope, wave drag, and drag-due-to-lift are nearly identical. The reverse delta wing has a large aerodynamic center shift as Mach number increases from subsonic to supersonic. Subsonic wind-tunnel tests were conducted with a variety of leading- and trailing-edge flap planforms to assess the longitudinal characteristics of a reverse delta wing. The experimental data show that leading-edge flaps are highly effective at increasing maximum lift and decreasing drag at moderate angles of attack. Trailing-edge flaps were up to 90% as effective as delta wing flaps in generating untrimmed lift increments.

Nomenclature

b	=	wingspan, in.
$b2$	=	wing semispan, in.
C_D	=	drag coefficient
C_{D0}	=	zero-lift drag coefficient
C_L	=	lift coefficient
C_m	=	pitching moment coefficient
c	=	local chord length, in.
c_p	=	pressure coefficient
DCL	=	lift coefficient increment
DF, df	=	trailing-edge flap deflection angle measured normal to hinge-line, deg
DN	=	leading-edge flap deflection angle measured normal to hinge-line, deg
M_∞	=	freestream Mach number
S_f	=	single flap reference area, in.^{2}
x	=	coordinate direction aligned with wing root chord, in.
y	=	coordinate direction toward wingtip, in.
α	=	angle of attack, deg
Λ_f	=	flap hinge-line sweep, deg

Introduction

SINCE the beginning of air travel, the goal has been to fly farther and faster. Twenty-five years ago, the Concorde demonstrated that commercial supersonic air travel was technically feasible. However, the aircraft has not been economically successful due to range restrictions, environmental concerns, and high operating costs. Today, increasing trans-Pacific traffic is creating a new high-speed transportation marketplace, thus motivating renewed interest in supersonic transport development. To compete in this marketplace, the U.S. is investing significant resources in the development of advanced technologies, principally in the areas of structures and propulsion. However, since the design studies of Boeing and Lockheed in the midsixties, little progress has been made in aerodynamics beyond detailed design refinement using modern CFD methods. Substantial vehicle improvements in cruise lift/drag ratio must be achieved to make supersonic flight more economically advantageous.

One method of attaining higher lift/drag ratio is through the substantial drag reductions achieved through maintaining laminar boundary-layer flow. If laminar flow can be achieved over large areas of a supersonic aircraft, transportation efficiency becomes comparable to subsonic airliners. Current efforts to obtain laminar flow are primarily directed towards stabilizing the laminar boundary layer by sucking a small quantity of boundary-layer air into the wing through porous skin surfaces. However, this approach is encumbered by a complex and costly suction system requiring porous wing skins, air collection ducts inside the wing, and suction compressors. The weight, suction drag and volume (wave drag) penalties negate much of the benefit of laminar flow skin friction drag reduction. The reliability and maintainability of the system are additional drawbacks.

The approach presented here is to provide conditions conducive to natural laminar flow (NLF) by utilizing a unique wing planform. NLF holds the promise of decreased system complexity and increased laminar flow coverage. NLF is inherently more robust because it depends entirely on a favorable wing flowfield. Types of vehicles to benefit from this technology include supersonic transports, supersonic business jets, long-range combat aircraft, and supersonic intercontinental cruise missiles.

The maintenance of a natural laminar boundary layer requires a flowfield of largely two-dimensional character. Significant lateral flow components, which are always present on conventional, highly swept delta wings, lead to crossflow instabilities causing transition to turbulent flow close to the leading edge. On the other hand, a delta wing flying in reverse direction, i.e., a wing planform with a straight leading edge and swept-forward trailing edges, exhibits largely two-dimensional flow at supersonic speeds. Thus, as shown in Fig. 1,

Received July 8, 1993; presented as Paper 93-3466 at the AIAA 11th Applied Aerodynamics Conference, Monterey, CA, Aug. 9–11, 1993; revision received May 3, 1994; accepted for publication May 3, 1994.

*Senior Engineer, Flight Mechanics Department, Advanced Technology and Design Center, 8900 East Washington Blvd. Member AIAA.

†Principal Engineer, Advanced Design Engineering, Advanced Technology and Design Center, 8900 East Washington Blvd. Associate Fellow AIAA.

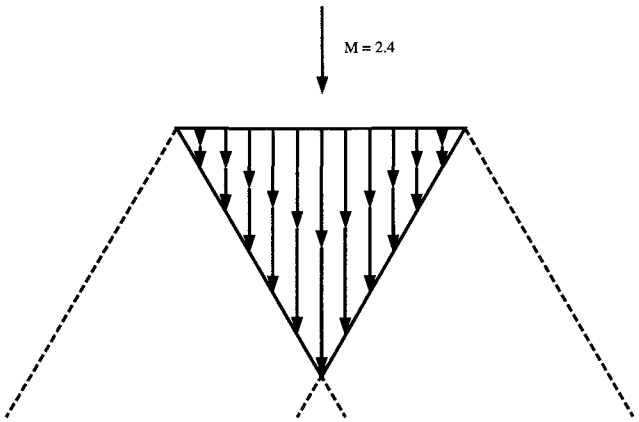

Fig. 1 Reverse delta wing with sonic trailing edges.

the reverse delta wing (with sonic trailing edges) is chosen as the basic wing planform in this approach to achieving NLF. The receding width of the wing geometry is an additional planform virtue, enabling large-percentage-area extents of laminar flow in the broad forward wing region.

The reverse delta wing with sonic trailing edges was originally derived by Busemann in his famous paper[1] presented at the Volta Congress in Rome, Italy in 1935. In this paper he introduced the swept-wing concept as a means to reduce supersonic drag. In elucidating one of these concepts he argued as follows: A straight wing of infinite span exhibits two-dimensional flow. On a straight wing of finite span, two-dimensional flow is preserved except in the triangular wingtip regions whose inboard boundary is given by the Mach line rays emanating from the forward wingtip corners. Truncating the wing at the Mach lines would not change the two-dimensional flowfield of the resulting wing. If the wingtips are cut off further and further inboard along Mach line rays, the rays finally intersect at the trailing edge of the original wing. What emerges is a wing having a straight leading edge and swept-forward trailing edges, i.e., the reverse delta wing with sonic trailing edges.

According to the reciprocal flow theorem for thin wings,[2,3] a reverse delta wing has the same wave drag and lift-curve slope as a delta wing of identical aspect ratio. Wave drag is related to the streamwise area distribution. Area distributions in forward and reverse direction are mirror images, and the drag integral taken in either direction is the same. The reciprocal flow theorem also holds true for drag-due-to-lift, provided the leading edges are supersonic in both orientations. However, because delta wings can have a subsonic leading edge, they can achieve leading-edge thrust. Thus, to show a net drag reduction, the increased extent of laminar flow on the reverse delta wing must provide a drag reduction that is greater than the drag penalty due to the loss of leading-edge thrust.

The large Reynolds numbers encountered by a full-scale supersonic transport wing at cruise conditions will not permit full-chord NLF. Transition via Tollmien-Schlichting (T-S) instability is likely to occur in the forward third of the wing surface. Laminar flow control (LFC) by cooling or thermal laminar flow control (TLFC) could be used to extend the range of laminar flow to the full wing surface.

TLFC is effective in stabilizing the laminar boundary layer against T-S disturbances, but does not significantly damp crossflow instability.[4] Thus, TLFC is applicable to reverse delta wings, but not to conventional delta wings in which boundary layer crossflow is the primary mode of transition. TLFC is very effective and efficient at supersonic speeds because aerodynamic heating provides a natural temperature gradient between the outer wing skin and fuel, which is taken aboard at ambient temperature. In addition, the fuel provides an abundant heat sink. Radiation is an additional, significant cooling mechanism that can be maximized by using special coatings of high IR emissivity and sunlight reflectivity.

NLF achieved on a reverse delta wing combined with wing cooling may represent a simpler, lighter approach than LFC by suction when applied to a conventional double delta wing. In addition, an LFC system based on wing surface cooling may displace less wing volume because it would require only a network of thin coolant pipes and small fuel circulation pumps that consume small amounts of power. The cooled wing surface may even allow the application of less exotic and expensive materials in the wing skin and structure.

Previous Work

Vincenti et al.,[5] in an early test of aspect ratio 2, 5% thick double-wedge section, triangular wings at Mach 1.53, confirmed the reversibility of supersonic flow described above to a first approximation. However, the disparate character of the lift distributions of conventional and reverse deltas was noted, as was the fact that lift-curve slope was slightly higher for the reverse delta. The difference was attributed to larger extents of adverse pressure gradient on the upper surface of the conventional delta that led to greater thickening or separation of the boundary layer near the trailing edge. Regarding minimum drag, the authors found their data inconclusive. On the one hand, they state that measured minimum drag was approximately independent of the direction of motion. But they also found evidence of significant support-body interference for the reverse deltas, thus precluding a definitive comparison. They noted that the pressure distribution characteristics of the reverse delta wing were conducive to the maintenance of NLF, and tests using the liquid-film technique confirmed the delay of transition. At a chord Reynolds number of 7.5×10^5, 20% of the delta wing surface was covered by turbulent flow, whereas only 6% of the reverse delta wing was turbulent. However, they had reservations as well: susceptibility to flow separation over the relatively blunt afterportion of the reverse delta wing, no possibility of improving lift-to-drag ratio through leading-edge suction, and large changes in aerodynamic center location when Mach lines from the tips intersect at off-design conditions.

Scope and Objective

This investigation was a first step in assessing the theoretical considerations discussed above. Inviscid delta wing and reverse delta wing flowfield characteristics at subsonic and supersonic Mach number were calculated using an Euler code. Chordwise pressure distributions and pressure contours are presented for both wings. Force and moment comparisons are made, and the applicability of reciprocal flow theory is addressed. No attempt was made to determine the effect of leading-edge thrust on the delta wing because its leading edge was assumed to be sharp and sonic. Likewise, the effect of boundary-layer transition location on skin friction drag, which is currently under investigation, will be reported in a future paper.

Low-speed wind-tunnel tests were conducted to assess general longitudinal characteristics of a reverse delta wing with particular emphasis placed on the effectiveness of a variety of leading- and trailing-edge flap planforms. A conventional delta wing was also tested for comparison. Flaps along the unswept trailing edge of a conventional delta wing operate efficiently because their hinge-lines are essentially normal to the flow. It was originally thought that trailing-edge flaps with highly swept hinge-lines, as one might envisage for a reverse delta wing, would be rather ineffective. The effectiveness was expected to diminish in proportion to cosine-squared of the hinge-line sweep angle. Thus, trailing-edge flap configurations were devised that would have greater effectiveness by virtue of reduced hinge-line sweep.

Computational Approach

Flowfield variables were calculated using the Northrop-developed Generalized Compressible Navier-Stokes (GCNSfv)

code[6] run in Euler mode. GCNSfv uses the diagonalized Beam-Warming algorithm of Pulliam and Steger[7] and a nodal finite volume discretization. The air was assumed to be a perfect gas with constant specific heats.

Aspect ratio 1.83, triangular wings with flat plate, 2% thick wedge, and 2% thick biconvex airfoils were analyzed. The computational grid was a single block, body-fitted, stacked-O mesh (H-O topology) with 101 streamwise points (41 along wing chord), 65 circumferential points around the span, and 49 points from the wing surface to the outer boundary. One grid was constructed such that the geometry could be analyzed in forward or reverse orientation. Delta wing leading edges and reverse delta wing trailing edges were swept to 65.38 deg, and were thus sonic at $M_\infty = 2.4$.

The supersonic cases ($M_\infty = 2.4$) were run at 0- and 4-deg angle of attack. Subsonic cases ($M_\infty = 0.2$) were run at angles of attack from 5 to 25 deg in increments of 5 deg.

Supersonic Computational Results

Surface Pressures

Euler calculations on a flat-plate reverse delta wing produce the perfectly two-dimensional, constant pressure field predicted by Busemann.[1] Upper surface pressure contours from Euler calculations on 2% thick reverse delta and delta wings at Mach 2.4 and 4-deg angle of attack are shown in Figs. 2a and 2b. Both wings have streamwise double-wedge sections. The flow direction is from left to right. The contours clearly show that strong spanwise pressure gradients occur near the leading edges of the delta wing (where they cause unfavorable conditions for boundary-layer stability). The reverse delta wing has two-dimensional flow with essentially zero pressure gradient fore and aft of the 50%-chord crest line.

Upper surface pressure contours from Euler calculations on reverse delta and delta wings with 2% thick biconvex airfoil sections are shown in Figs. 3a and 3b. Again, the Mach number is 2.4 and the angle of attack is 4 deg. A reverse delta wing with streamwise biconvex sections produces a supersonic expansion (decreasing pressures) in the streamwise direction. This favorable pressure gradient increases the stability of the (natural) laminar boundary layer by inhibiting the growth of the Tollmien-Schlichting wave disturbances. Since the isobars are swept, the favorable chordwise pressure gradient will cause a small spanwise pressure gradient leading to crossflow instabilities in the boundary layer. However, Navier-Stokes analysis performed at Northrop has shown that the crossflow Reynolds number is subcritical except in a narrow region near the trailing edge. Isobars on a delta wing with streamwise biconvex sections have a highly three-dimensional character in the leading-edge region that is substantially similar to that shown in Fig. 2b.

Chordwise upper and lower surface pressure distributions at different spanwise locations on the reverse delta wing with biconvex sections are shown in Fig. 4. Compression occurs on the lower surface at the leading-edge shock, but the remainder of the lower surface and all of the upper surface are exposed to supersonic expansion, i.e., favorable pressure gradients, with the exception of a small region near the trailing edge. These pressure distributions are nearly identical to those predicted from linear supersonic thin airfoil theory, providing additional evidence of the two dimensionality of the flow.

In contrast, delta wing chordwise surface pressure distributions shown in Fig. 5 reveal a large adverse pressure gradient on the upper surface in the leading-edge region. This gradient will amplify instabilities and promote strong boundary-layer crossflow on a swept wing. A delta wing with a more

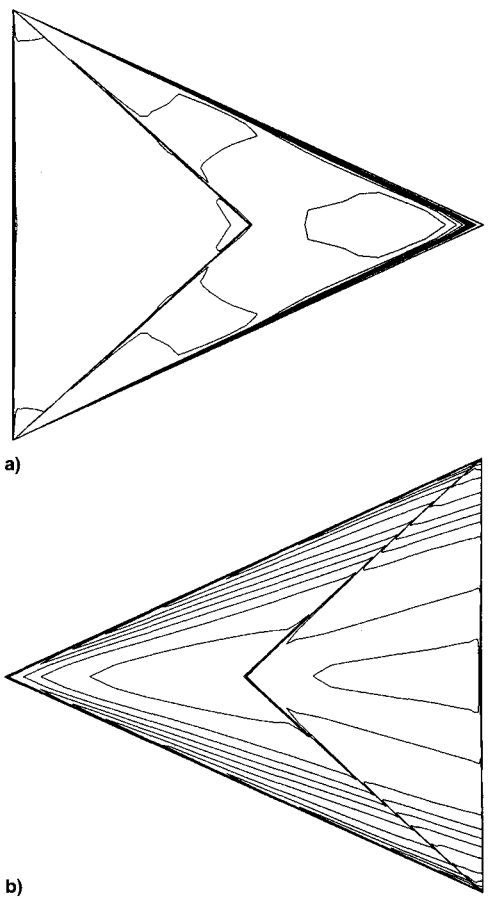

Fig. 2 Pressure coefficient contours on 2% thick wings with streamwise double-wedge sections ($M_\infty = 2.4$, $\alpha = 4$ deg). Flow direction from left to right. Contour increment = 0.0114: a) reverse delta wing and b) delta wing.

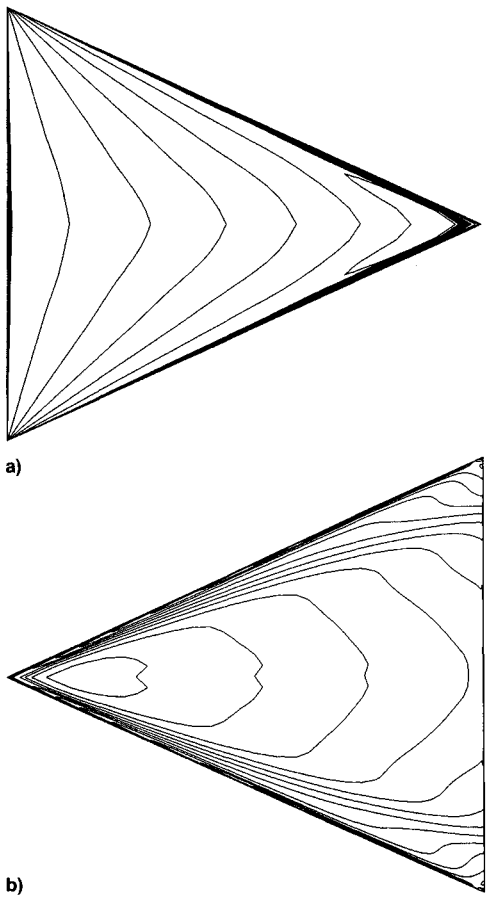

Fig. 3 Pressure coefficient contours on 2% thick wings with streamwise biconvex sections ($M_\infty = 2.4$, $\alpha = 4$ deg). Flow direction from left to right. Contour increment = 0.0114: a) reverse delta wing and b) delta wing.

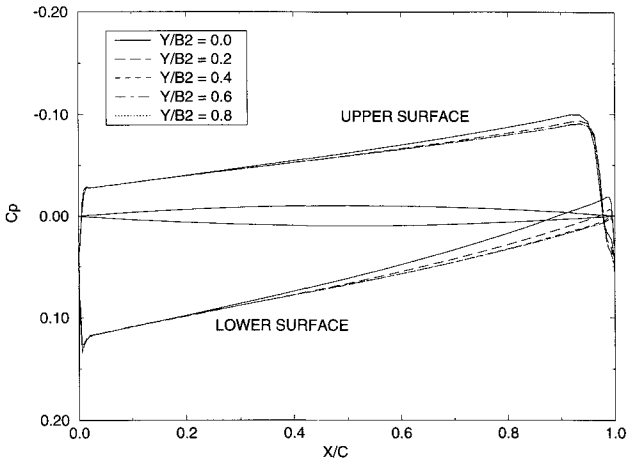

Fig. 4 Reverse delta wing chordwise pressure distributions (M_∞ = 2.4, α = 4 deg).

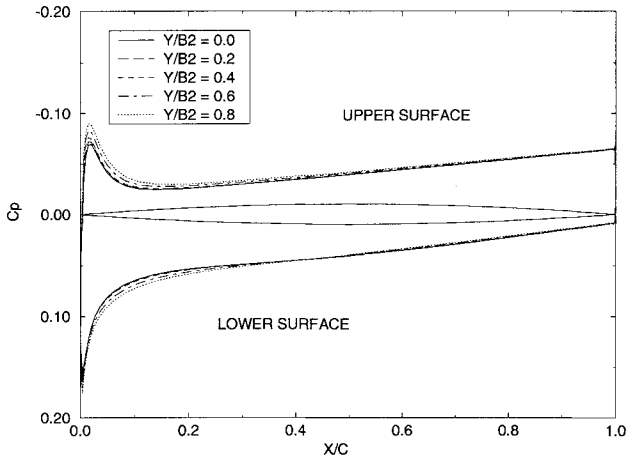

Fig. 5 Delta wing chordwise pressure distributions (M_∞ = 2.4, α = 4 deg).

highly swept, subsonic, rounded leading edge would be expected to have even more severe crossflow in addition to attachment line instability.

Forces and Moments

Longitudinal forces and moments were calculated for the 2% thick biconvex-section delta and reverse delta wings at 4-deg angle of attack and Mach 2.4 by integrating surface pressures from the Euler solutions; no attempt was made to estimate viscous effects. The lift-curve slope of each wing is 0.030/deg, similar to the linear two-dimensional value of 0.032/deg. Delta wing aerodynamic center is located at 48.5% mean aerodynamic chord (m.a.c.) while reverse delta wing aerodynamic center is located at 45.0% m.a.c. (the linear two-dimensional value is 50% m.a.c. in both cases).

Zero-lift wave drag for the two wings is almost identical as predicted by reciprocal flow theory. The Euler code predicts zero-lift wave drag values of 11.6 counts for the reverse delta wing and 10.0 counts for the delta wing. The linear two-dimensional value is 9.8 counts. Of course, the wave drag of an aircraft does not depend on the wing alone. The vehicle wave drag is related to the overall volume distribution that is constrained by volumetric constraints such as landing gear stowage, fuel volume, structural efficiency, etc. The consequences of integrating a reverse delta wing into a configuration must therefore be considered, and that study will be discussed in a future paper. The drag-due-to-lift (induced drag plus wave drag-due-to-lift) of the reverse delta wing at 4-deg angle of attack is 83.6 counts—exactly equal to the two-dimensional prediction given by $C_L \times \alpha$. The drag-due-to-lift of the delta wing is 80.4 counts.

Experimental Approach

Low-speed tests were conducted in the Northrop Research Wind Tunnel during October 1992. This facility is a closed-circuit, single-return, continuous flow tunnel operating at atmospheric static pressure. The cross-sectional area of the test section is 0.7 × 1.0 m. All tests were conducted at a Mach number of 0.2, dynamic pressure of 60 lb/ft^2, and unit Reynolds number of 1.4 × 10^6/ft. Most tests were performed with variations of the reverse delta baseline wing, but a small number of tests with the delta wing were conducted as well. Data was acquired at angles of attack up to 55 deg.

The models tested were $\frac{1}{16}$-in.-thick, flat-plate, aspect ratio 2 triangular wings with a root chord of 1.0 ft. No edge treatment, i.e., beveling, rounding, etc., was applied. Tests performed with sharpened leading edges on the reverse delta and delta models showed these effects to be minor. A thin vertical plate with a length equivalent to the root chord was attached at the centerline to act as a stiffener. The models were sting-mounted to the support system and a fairing, or sting shroud, covered the balance. Due to the forward position of the aerodynamic center of the reverse delta, the nose of the sting shroud was even with the wing's leading edge. A test with the model inverted indicated only a minimal sting-shroud interference effect. Two leading-edge and six trailing-edge flap shapes were tested on the reverse delta wing; one trailing-edge flap shape was tested on the delta wing. Illustrations of

Table 1 Control surface descriptions

Control surface	Type	Λ_f, deg	S_f, in.^{2}	$\cos^2\Lambda_f$
Reverse delta				
LE flap 1	Constant percent chord	17.0	4.68	0.9145
LE flap 2	Constant chord	0.0	4.22	1.0000
TE flap 1	Constant percent chord	55.0	5.17	0.7573
TE flap 2	Constant chord	63.4	5.17	0.2005
TE flap 3	Inverse taper	73.0	5.08	0.0855
TE flap 4	Dual trailing-edge flaps	40.0	5.76	0.5868
TE flap 5	Dual trailing-edge flaps	0.0	5.76	1.0000
Delta				
TE flap 7	Constant chord	0.0	4.22	1.0000

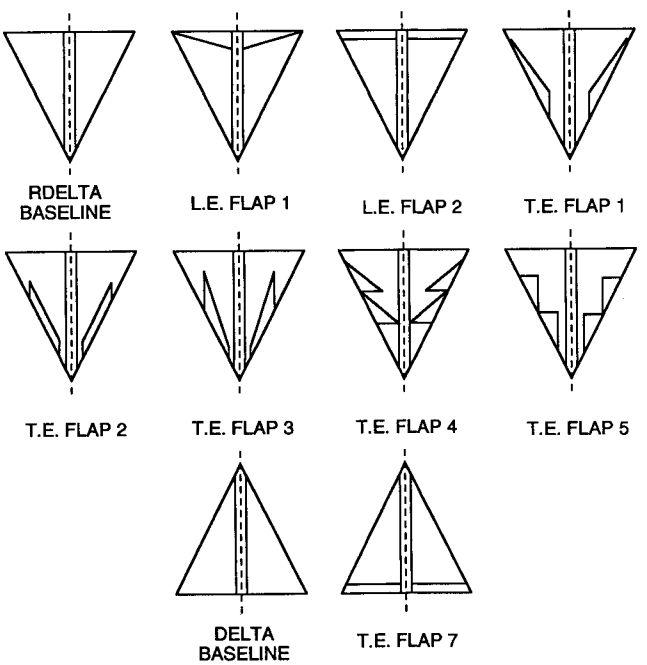

Fig. 6 Test models and flap planform nomenclature.

all control surfaces are shown in Fig. 6, with descriptions in Table 1. Two leading-edge flap deflection angles and three trailing-edge flap deflection angles were tested. Flap deflection angles were measured normal to the hinge-line.

Experimental Results

Comparisons of delta and reverse delta wing longitudinal characteristics at Mach 0.2 are shown in Figs. 7a–7c. The solid lines represent wind-tunnel data and the discreet points are from Euler calculations. In the following discussions, a note of caution is in order so that high angle-of-attack data are interpreted in the proper context. The research tunnel described previously is a diagnostic tunnel with limited high angle-of-attack capability. Since the test section area is not large, and since Reynolds number is low in comparison to those expected in flight, absolute values of maximum lift are not reliable. However, increments in maximum lift due to configuration changes are believed to be accurate. Because both wings have a low aspect ratio, maximum lift occurs at angles of attack that are immaterial to transport aircraft flight profiles. The angles of attack that are of interest for this class of aircraft are usually less than about 15 deg due to considerations of tail strike on takeoff and passenger comfort. Nevertheless, wind-tunnel data through about 30-deg angle of attack are presented in this study for completeness.

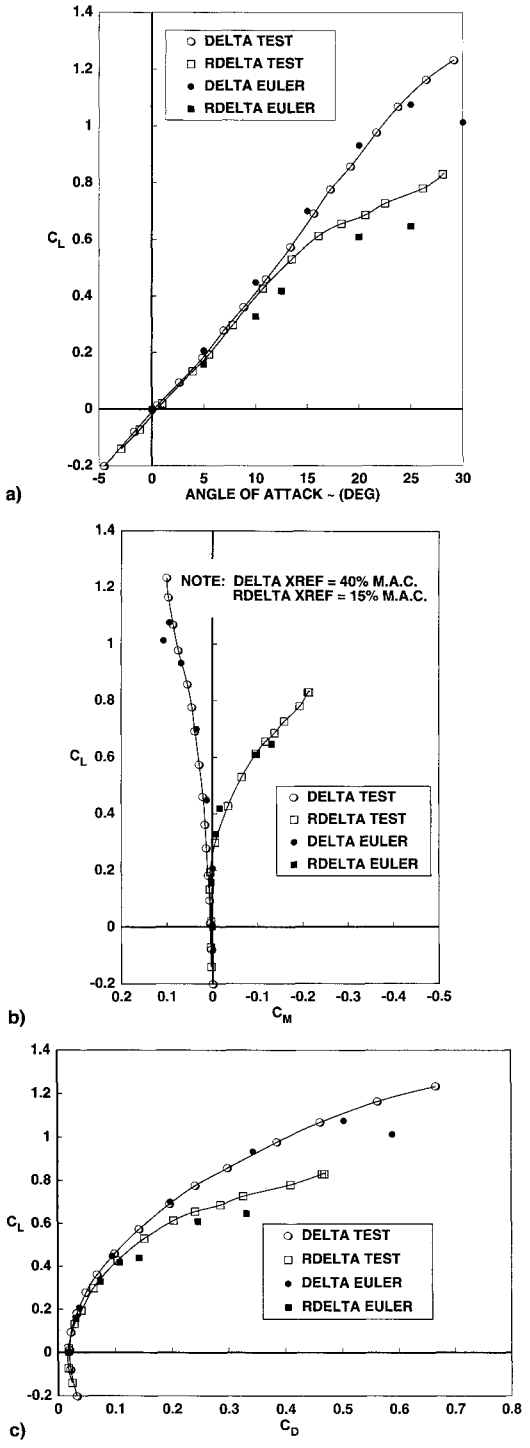

Fig. 7 Longitudinal characteristics of delta and reverse delta wings (M_∞ = 0.2). Lift coefficient as a function of a) angle of attack, b) pitching moment coefficient, and c) drag coefficient.

The data in Fig. 7a indicate that lift-curve slope is independent of the direction of motion at low angles of attack. At moderate angles of attack, reverse delta wing lift-curve slope decreases due to the onset of large-scale viscous separation. A gentle, benign stall begins at about 16-deg angle of attack. The delta wing lift curve displays the typical increase in slope due to leading-edge vortex formation.

Figure 7b is a plot of lift vs pitching moment with reference points at 40% m.a.c. (60% root chord) for the delta and at 15% m.a.c. (10% root chord) for the reverse delta wing. Both show benign characteristics, and the reverse delta wing trend is toward additional stability at high angles of attack. The reverse delta wing shows signs of substantial stall and departure resistance at higher angles of attack not shown in the plot. The aerodynamic centers of the delta wing and reverse delta wing as given by test data are 38.1% and 11.8% m.a.c., respectively, and by the Euler calculations are 40.1% and 13.2% m.a.c., respectively. The extreme forward location of the reverse delta aerodynamic center is typical for wings of this shape.[8] Subsonically, a reverse delta wing is highly loaded in the broad forward wing region. For this reason, leading-edge flaps are very effective as discussed below.

A substantial shift of 31.8% m.a.c. in reverse delta wing aerodynamic center location occurs between subsonic and supersonic regimes (recall that the aerodynamic center at Mach 2.4 was 45.0% m.a.c.). In contrast, the delta wing aerodynamic center shifts 8.4% m.a.c. between regimes. The large aerodynamic center shift has several ramifications for an aircraft with a reverse delta wing. Compensation for the change in stability using means such as control surfaces deflected proportional to angle of attack, fuel management, and stability augmentation by a rapid-action control surface is required. Large trailing-edge flap deflections can be used for trimmed subsonic flight at negative stability. The resulting high-lift coefficients improve takeoff and landing performance compared to delta wings where the trailing-edge flap deflections are typically trim-limited.

Drag comparisons are shown in Fig. 7c. The Euler data in the plot have been offset by the experimental value of C_{D0} to facilitate pressure drag comparisons. The test model reverse delta wing exhibits higher total drag at the moderate-to-high angles of attack. Euler calculations show the same trend (partially due to numerical viscosity). A flow-visualization test with yarn tufts was performed using the reverse delta wing, and separation was seen to begin in the leading-edge region at low angle of attack and spread from root to tip with increasing angle of attack. Much of the reverse delta wing excess drag is thus due to viscous form drag. In addition, it is well known[9] that wings with raked-in tips suffer an induced drag penalty due to a lower "effective" aspect ratio, i.e., a decreased "vortex span." Most of these adverse effects will be mitigated by leading-edge devices.

Figures 8a–8c show the flap planform effect of constant-percent-chord and constant-chord leading-edge flaps deflected 34 deg. Figure 8a indicates that both leading-edge flaps increase the maximum usable lift of the reverse delta wing by about 10%. In addition, stall is delayed by increasing the usable angle of attack by 8 deg. As shown in Fig. 8b, deflection of each flap planform results in constant aerodynamic center position for a larger angle-of-attack range. The pitching mo-

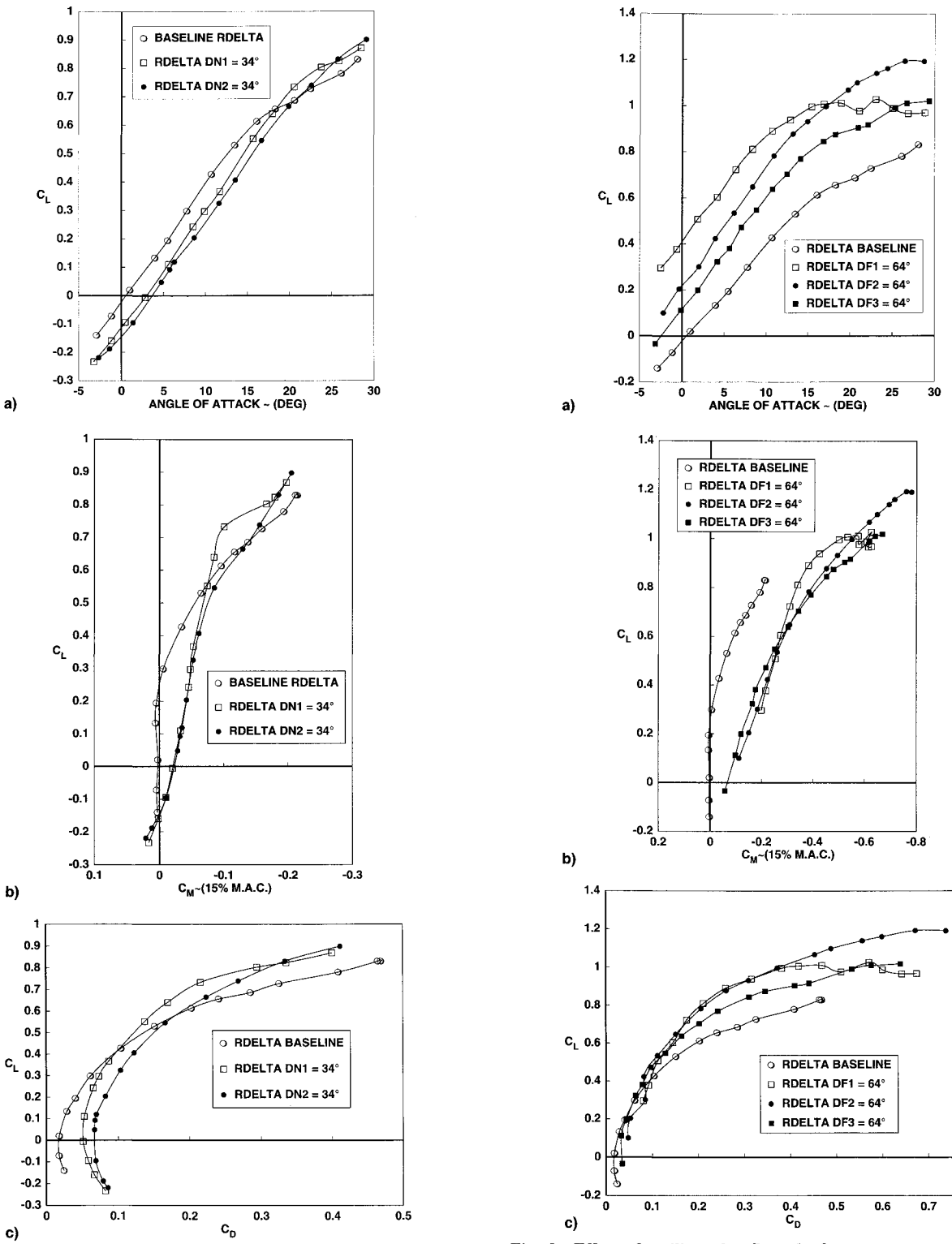

Fig. 8 Effect of leading-edge flap planform on reverse delta wing longitudinal characteristics ($M_\infty = 0.2$). Lift coefficient as a function of a) angle of attack, b) pitching moment coefficient, and c) drag coefficient.

Fig. 9 Effect of trailing-edge flap planform on reverse delta wing longitudinal characteristics ($M_\infty = 0.2$). Lift coefficient as a function of a) angle of attack, b) pitching moment coefficient, and c) drag coefficient.

ment data in Fig. 8b also indicate a stabilizing 12.7% m.a.c. shift in the aerodynamic center location. Leading-edge flaps on conventional wings usually add a camber effect only and, thus, do not contribute to a wing's stability. The data in Fig. 8b suggest that leading-edge flaps on a reverse delta wing may have the unique characteristic of enabling control of the subsonic aerodynamic center position. Figure 8c shows that drag is markedly reduced by deflecting leading-edge flaps. The constant-percent-chord flap planform appears to be more effective at generating favorable lift, pitching moment, and drag characteristics.

A comparison of the effects of constant-percent-chord, constant-chord, and inverse-tapered trailing-edge flap planform is shown in Figs. 9a–9c. As expected from hinge-line sweep considerations, the constant-percent-chord flap produces the largest lift increment at angles of attack less than 17 deg as shown in Fig. 9a. The constant-chord flap was more effective at higher angles of attack. Like the leading-edge flap data, the data presented in Fig. 9b show that there is also a signif-

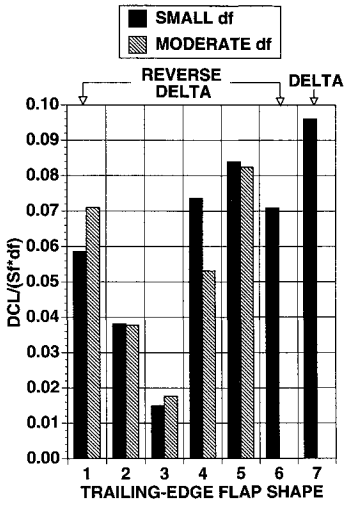

Fig. 10 Normalized trailing-edge flap effectiveness.

icant stabilizing shift in the aerodynamic center when trailing-edge flaps are deflected to 64 deg. As shown in Fig. 9c, the drag polar is markedly improved, particularly by the constant-percent-chord and constant-chord flaps.

Comparisons of relative lift increments produced by different flap planforms shown in Figure 9a should be made with caution since the only parameter held constant is the flap deflection angle. Reference should be made to Table 1 in which flap planform areas and flap hinge-line sweeps are given. From a fundamental point of view, the most desired flap shape is the one that produces the greatest lift increment for the least amount of surface area and deflection. Consequently, Fig. 10 was prepared that shows normalized "flap effectiveness" for all reverse delta wing trailing-edge flaps (trailing-edge flaps 1–6) as well as the one delta wing trailing-edge flap (trailing-edge flap 7) that were tested. In the figure, "small d_f" refers to deflection angles around 30 deg, whereas "moderate d_f" refers to deflection angles around 60 deg. Lift increments (DCL in the figure) were determined at an angle of attack of 15 deg. As expected, the trailing-edge flap of the delta wing is the most effective according to the aforementioned definition. Reverse delta trailing-edge flap shapes 1, 4, 5, and 6 are 65–90% as effective at producing lift increments per deflection angle and per planform surface area. Theoretically, the trend should inversely follow the cosine squared of the hinge-line angle, yet trailing-edge flap 1 is as effective as trailing-edge flap 4, even though its hinge-line is swept 15 deg more.

The flaps with an unswept hinge-line tend to stall at relatively small deflections, whereas flaps with swept hinge-lines stall at rather large deflections. This characteristic of the swept hinge-line flap is used to advantage when large flap deflections are utilized to trim an unstable reverse delta configuration.

Another measure of the utility of a particular flap planform is the amount of pitching moment required to trim the aircraft when flaps are deflected. Trim drag decreases and pitch control surfaces can be smaller if flap-induced pitching moment is less. Calculations show that overall, trailing-edge flap 4 produces the minimum pitching moment increment for a given lift increment, whereas trailing-edge flap 1 is optimum among the single flap shapes. Trailing-edge flap 3 gives the largest values of $\Delta C_m/\Delta C_L$. In comparison, trailing-edge flap 7 on the delta wing is not good either, which suggests an additional benefit of the reverse delta concept: Because the centroid of the additional lift due to flap deflection is closer to the vehicle c.g., less down force will be required to trim; thus, trim lift-loss and trim drag will be less.

Conclusions

Euler analyses were conducted to assess and compare the aerodynamic characteristics of delta and reverse delta wings at subsonic and supersonic Mach numbers. The data presented in this report confirm that the flow over a reverse delta wing is nominally two dimensional, in contrast to delta wing flow that exhibits large spanwise flow gradients, particularly near the leading edge. The data suggest that crossflow and attachment line instabilities, the primary modes of transition on swept wings, are thus minimal on a reverse delta wing.

Inviscid force calculations at supersonic Mach number indicate equal lift-curve slope for delta and reverse delta wings. Both wings had nearly the same wave drag and drag-due-to-lift, corroborating the principles of reciprocal flow theory. The analysis quantified a large subsonic-to-supersonic aerodynamic center shift for the reverse delta wing.

Subsonic wind-tunnel test results established the benign character of reverse delta wing aerodynamics. The following observations summarize the subsonic results presented in this article.

1) In the angle-of-attack range relevant to a transport aircraft flight regime, lift-curve slope is independent of the direction of motion. The clean delta wing attains higher maximum lift, albeit at very high angle of attack.

2) Leading-edge flaps were effective at decreasing reverse delta wing drag and increasing lift at moderate to high angles of attack.

3) Respectable reverse delta lift increments were obtained using trailing-edge flaps. It was found that the best reverse delta flaps could obtain up to 90% of the lift-increment effectiveness of delta wing flaps.

4) Large deflections of leading- and trailing-edge flaps shift the aerodynamic center aft—a favorable characteristic for a wing with a large subsonic-to-supersonic aerodynamic center shift.

5) Flap-induced pitching moments were found to be much less severe for the reverse delta wing.

References

[1]Busemann, A., "Aerodynamischer Auftrieb bei Überschallgeschwindigkeit," *Luftfahrtforschung*, 1935, p. 210.

[2]Von Karman, T., "Supersonic Aerodynamic Principles and Applications," *Journal of the Aeronautical Sciences*, Vol. 14, No. 7, 1947, p. 382.

[3]Jones, R. T., *Wing Theory*, Princeton Univ. Press, Princeton, NJ, 1990, pp. 149–161.

[4]Lekoudis, S., "The Stability of the Boundary Layer on a Swept Wing with Wall Cooling," *AIAA Journal*, Vol. 8, No. 9, pp. 1032–1034.

[5]Vincenti, W. G., Nielsen, J. N., and Matteson, F. H., "Investigation of Wing Characteristics at a Mach Number of 1.53. I—Triangular Wings of Aspect Ratio 2," NACA RM-A7I10, Dec. 1947.

[6]Lonergan, L. A., "A Description of the Generalized Compressible Navier-Stokes Code (GCNSfv) Methodology," Northrop Internal Memorandum T233-93-015, April 1993.

[7]Pulliam, T. H, and Steger, J. L., "Implicit Finite-Difference Simulations of Three-Dimensional Compressible Flow," *AIAA Journal*, Vol. 18, No. 1, 1980, p. 159.

[8]Heaslet, M. A., and Spreiter, J. R., "Reciprocity Relations in Aerodynamics," NACA Rept. 1119, 1953, p. 11.

[9]Hoerner, S. F., *Fluid-Dynamic Drag*, Hoerner Fluid Dynamics, NJ, 1965, pp. 7-6–7-17.